Electrochemistry of catalase at a liquid|liquid micro-interface array

Shaheda Zannah and Damien W. M. Arrigan*
Curtin Institute for Functional Molecules and Interfaces, School of Molecular and Life Sciences, Curtin University, GPO Box U1987, Perth, Western Australia, 6845, Australia.

* Author for correspondence Email d.arrigan@curtin.edu.au

Abstract

The electrochemistry of catalase (CAT) was investigated at the interface between two immiscible electrolyte solutions (ITIES) as step towards its non-redox detection. Electrochemistry at the ITIES offers advantages such as the non-redox detection of biomolecules. The electrochemical behaviour of CAT at the ITIES, in a micro-interface array format displayed a distinct cyclic voltammogram when the aqueous phase pH was lower than the isoelectric point (pI) of CAT. No voltammetric response was observed when the aqueous phase pH > pI of CAT indicating that neutral or negatively charged CAT has no capability to facilitate anion transfer from the organic phase. Adsorptive stripping voltammetry (AdSV) was assessed for detection of low concentrations at the μITIES array. Application of a positive preconcentration potential for a fixed time enabled interfacial accumulation of CAT as a complex subsequently, a voltammetric scan to lower potentials desorbed the complex, providing the electroanalytical signal. Assessment of sample matrix effects by examining the electrochemistry of CAT in artificial serum indicated that detection in pH-adjusted samples is feasible. Together, these results demonstrate that CAT is electroactive at the liquid-liquid interface and this may be useful as a strategy to detect and characterize the enzyme in a label-free manner.

Keywords: Catalase, micro-interface, voltammetry, adsorption, ITIES

1. Introduction

Catalase (CAT) is an antioxidant enzyme (EC 1.11.1.6) that plays an important role in the defence mechanism against oxidative stress by neutralizing reactive oxygen species (ROS) by converting hydrogen peroxide into water and oxygen (H_2O_2 into H_2O and O_2) [1]. CAT is a tetramer, composed of four alike subunits, and functions in two ways: catalytically by decomposing hydrogen peroxide into water and oxygen, and peroxidatively, by oxidizing various metabolites and toxins such as formaldehyde, alcohol, formic acid, phenols, acetaldehyde, or nitrite using H_2O_2 [2, 3]. Each CAT monomer has a haem group, iron (III) protoporphyrin IX, at its redox active centre and a bound nicotinamide adenine dinucleotide phosphate NADP group [4, 5]. Catalase has unit cell dimensions of 67.8 Å × 172.1 Å × 182.1 Å, as determined by microcrystal electron diffraction [6], with a hydrodynamic radius of 5.2 nm [7] and a molecular weight of 250 kDa [8]. Its isoelectric point is 5.4 [9], so that at physiological pH it is anionic. This enzyme is found in almost all aerobic organisms and in the cellular organelles of humans where it takes part in protecting against oxidative damage by ROS [10]. CAT is also found in some anaerobic microorganisms [11] and is ubiquitous amongst plants and liable for fungal growth and cell proliferation in most fungi [12]. Several studies showed that altered CAT expression is responsible for a number of pathophysiological conditions in humans. For example, the mutation of CAT genes has been associated with certain diseases, like Alzheimer's disease, diabetes mellitus, vitiligo, hypertension, and CAT deficiency is the causal effect of Acatalasemia [13, 14]. CAT expression has been found in a number of studies to be downregulated in human tissues compared to normal tissues [15, 16]. CAT deficiency has also been associated with Wilson's disease, cardiovascular disease, anaemia, and some dermatological disorders [12]. In point of fact, ROS are responsible for activating many signalling pathways that help the proliferation, migration and capture of cancer cells. CAT can inhibit these deadly processes simply by detoxifying ROS, particularly H_2O_2, into less reactive oxygen and water [17]. According to some research results, CAT and superoxide dismutase are able to control the migration and uncontrolled proliferation of cancer cells [15]. However, a number of studies have indicated that CAT is a biomarker, such as in thyroid disorders where the CAT level was found to be overexpressed [18]. CAT can be considered as a biomarker as its upregulation and downregulation can be a diagnostic or prognostic indicator for identifying and monitoring of a particular disease, although it has not been approved by regulatory authorities nor undergone clinical trials for this. CAT has been extensively studied by electrochemistry at solid electrodes where its redox activity was examined [2, 10, 19, 20] but its electrochemistry at liquid-liquid interfaces has not been reported, which is the purpose of this study.

Here in this report, the electrochemical behaviour of CAT at the liquid-liquid (L/L) interface formed in a micro-array was investigated. Electrochemistry at the L/L interface, or at the interface between two immiscible electrolyte solutions (ITIES), is predominantly based on ion transfers from one electrolyte solution to the other. This process does not inevitably need any oxidation/reduction associated with the transferring ions but a process involving charge transfer of either ions or electrons (or both) [21, 22] allows the study of the electrochemical behaviour of a range of ions or ionisable (bio)molecules. It has several advantages over conventional electrochemical systems, such as easy tailoring of organic and aqueous phases, versatility for detection of target analytes, simplification of the electrochemical cell, easily controlled process of miniaturization and, more importantly, label-free detection feasibility [23]. It has immense applications in broad areas like the detection of biomolecules and ionised species, drug release and delivery, solvent extraction, electrochemical biosensor development, and biological membrane simulation [24, 25]. There is on-going interest in the electrochemical behaviour of drugs [26], amino acids [27], and a variety of biomacromolecules (e.g. haemoglobin [28], myoglobin [29], lysozyme [30], insulin [31], cytochrome c [32], acid phosphatase [33], oligopeptides [34]) at the ITIES. A recent study exemplified the use of such electrochemistry in protein immobilisation by examining the electrochemically-driven co-deposition of three proteins (haemoglobin, acid phosphatase and α-amylase) and silica film at the ITIES for selective protein analysis [35].

In this study, CAT has been considered as a model enzyme as a step towards the detection of enzymatic biomarkers using L/L electrochemistry. The term biomarker was first used in 1989 as an indicator of some levels or biological conditions which can be quantified [36]. According to The World Health Organization (WHO), a biomarker is "any substance, structure, or process that can be measured in the body or its products

and influence or predict the incidence or outcome or disease" [37]. A biomarker has immense applications and can be used as a diagnostic, prognostic, risk measurement, safety, pharmacodynamic/response, and/or predictive indicator [38, 39]. As a result, it is very useful to measure biomarkers at an early onset of a particular disease to improve the patient's health condition and overall survival rate. Along with other available techniques electrochemical strategies are used a lot to detect and measure biomarkers as these techniques offer simplicity, low cost, fast response, reliability, robustness, and low chances of false result [40]. A prostate cancer biomarker, prostate specific membrane antigen (PSMA), has been detected efficiently at picomolar concentrations employing voltammetry at a μITIES array [41].

This work presents the investigation into the electrochemical behaviour and detection of CAT as a model enzyme biomarker using a L/L μinterface array with cyclic voltammetry and adsorptive stripping voltammetry. This study would be very helpful in detecting any enzymatic biomarkers in a simple, low cost manner without expensive labelling or antibodies, and in a fast way to make it advantageous for use in diagnostics. This sensitive non-redox electrochemical method offers advantages in examining biologically important macromolecules in an efficient way.

2. Experimental methods

2.1. Reagents

Lyophilized powder catalase from bovine liver (2000 – 5000 units/mg protein) with molecular weight (MW) 250,000 Da [8] was purchased from Sigma-Aldrich and used as received. All other reagents were purchased form Sigma-Aldrich and used as received unless stated otherwise. The organic phase electrolyte salt bis(triphenylphosphoranylidene)ammonium tetrakis(4-chlorophenyl)borate (BTPPATPBCl) was prepared by metathesis of equimolar amounts of bis(triphenylphosphoranylidene)ammonium chloride (BTPPACl) and potassium tetrakis(4-chloropheynl)borate (KTPBCl). BTPPATPBCl was prepared at 10 mM in 1,2-dichloroethane (1,2-DCE). The reference solution for the organic phase reference electrode was aqueous 1 mM BTPPACl in 10 mM LiCl. All aqueous phase electrolytes were prepared using purified water (resistivity: 18.2 MΩcm) from a USF Purelab with UV system. A stock solution of CAT was prepared at 0.1 mM in 10 mM phosphate buffered saline (PBS) on a daily basis. For experiments involving ion transfer of tetraalkylammonium ions like tetraethylammonium (TEA^+) in the presence of CAT, the stock solution of TEA^+ was prepared at 10 mM in 10 mM LiCl.

2.2. Apparatus

Electrochemical measurements were conducted with either an AUTOLAB PGSTAT101N or an AUTOLAB PGSTAT302N electrochemical workstations (Metrohm, The Netherlands) operated with the supplied NOVA software. Voltammetry was performed with μITIES arrays prepared from glass membranes consisting of 100 microholes (10 x 10 square array) laser ablated in a circular borosilicate glass membrane of ~130 μm thickness [42]. The diameters of the microholes were larger on the laser entry side than on the laser exit side of the membranes (diameters of the respective microholes are illustrated in Schematic 1). In all cases, one side of the glass membrane was functionalised with (1H,1H,2H,2H-perfluorooctyl)silane to make it hydrophobic. The micro-interfaces were formed at either the laser exit side (used in experiments for simple ion transfer in presence of CAT) or the laser entry side (used for all other experiments). The glass membrane was glued to a glass tube (~5.3 mm internal diameter) with glass silicone (Selley, Australia and New Zealand) with the hydrophobic side of the membrane facing the glass cylinder so the organic solvent can be placed inside it and consequently inside the microholes, and inner walls of the pores were also hydrophobic. The silicone was allowed to cure for 24 h and the assembly was subsequently rinsed with acetone and dried in air before electrochemical experiments. The organic phase (~200 μL) was first placed into the glass tube with attached glass membrane to aid the filling of the microholes with the organic phase. Then on the top of organic phase, the organic reference solution was added [42]. This set-up was then inserted into the aqueous phase and two Ag/AgCl reference electrodes (one in each phase) were used to complete the cell, as described in Schematic 2.

2.3. Electrochemical measurements

Cyclic voltammetry (CV) and linear sweep adsorptive stripping voltammetry (AdSV) were carried out at a sweep rate 5 mV/s, unless indicated otherwise. Parameters such as protein concentration, potential applied, sweep rate and preconcentration time were varied as required. All experiments were implemented three times and average values were taken for analysis. In these experiments, a positive current corresponds to cation transfer from the aqueous to organic phase or anion transfer from organic to aqueous phase, and a negative current corresponds to anion transfer from aqueous to organic phase or cation transfer from organic to aqueous phase [22].

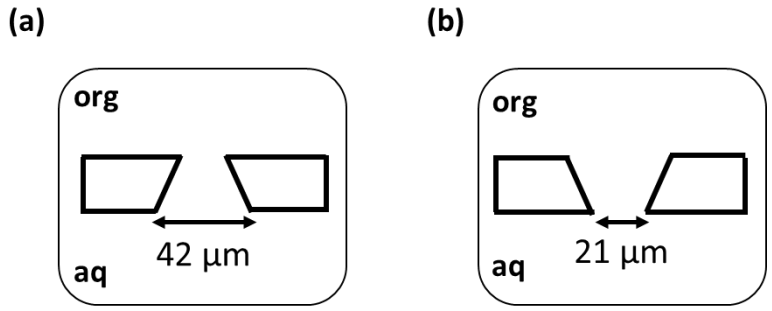

Schematic 1. Sketch of microholes in glass membranes showing the microhole diameters, with (a) microholes of wider diameter located at laser entry side and (b) microholes of narrower diameter located at laser exit side.

$$\mathbf{Ag}\,\big|\,\mathbf{AgCl}\,\big|\,\begin{matrix}\mathbf{1\ mM\ BTPPA^{+}Cl^{-}}\\ \mathbf{in\ 10\ mM\ LiCl}\end{matrix}\,\big|\,\begin{matrix}\mathbf{10\ mM\ BTPPA\,TPBCl}\\ \mathbf{in\ 1,2\ DCE}\end{matrix}\,\big\|\,\begin{matrix}\mathbf{10\ mM\ HCl\ /\ LiCl\ /\ PBS}\\ \mathbf{or\ AS\ +\ x\ \mu M\ CAT}\end{matrix}\,\big|\,\mathbf{AgCl}\,\big|\,\mathbf{Ag}$$

Schematic 2. Schematic representation of electrochemical cell employed where x denotes the concentration of CAT used in the study. CAT is catalase, PBS is phosphate buffered saline, AS is artificial serum.

3. Results and discussion

3.1. Cyclic voltammetry of CAT in different aqueous phase conditions

An initial investigation was carried to examine the electrochemical activity of CAT at the µITIES array using cyclic voltammetry (CV). CV was employed with different aqueous phase pHs to determine the impact of pH on CAT electroactivity. Figure 1 shows the distinct voltammogram of CAT at the µITIES array using cell 1 (Schematic 2). The CVs shown in Figure 1 are all the third cycle of the experimental set-up, as it was found that currents changed on repeated cycling (see Supplementary Information Figure S1 for CVs of 1st, 3rd and 8th cycles at each aqueous phase pH studied); selecting the 3rd cycle for study was based on obtaining a reproducible signal between different cell set-ups and time involved in the experiment. At pH 2 (aqueous phase 10 mM HCl), a well-defined CV for 2 µM CAT was recorded (Figure 1(a)). Upon scanning from lower towards higher potentials, a clear forward peak was observed at 0.61 V accompanied by a small post-peak, while scanning in the reverse direction produced a narrow sharp peak at 0.47 V. Together, this CV indicates that CAT is electrochemically active at the µITIES array in acidic conditions. But at aqueous phase of pH 5.5 (the natural pH of 10 mM LiCl), no obvious CV response was observed (Figure 1(b)), on comparison of CVs in the absence (black dashed line) and in the presence of 2 µM CAT (black solid line). In respect of this observed pH dependence, CAT behaves like other proteins at the ITIES, e.g. ferritin [43], insulin [44], lysozyme [44], myoglobin [29], haemoglobin [45], where below the pI of CAT (pI 5.4) [9]; it is protonated and cationic in nature. But when the aqueous phase pH is higher than the pI of CAT, it is anionic in nature and no definite voltammetric response was found. A similar result was found when the aqueous phase was 10 mM PBS (pH 7) and no voltammetric response was found in presence of 1 µM CAT (Figure 1(c)). Based on these findings, it can be inferred that CAT is detectable and is electroactive at the µITIES array when it is protonated [28, 44, 45]. At pH 2, below the isoelectric point of CAT, it is assumed to have 80 positive charges, based on its amino acid sequence and assuming every ionisable functional group is protonated. In addition to the pH dependence, the other notable feature of these CVs is their peak shape. Based on the use of a µITIES array, for a simple diffusion controlled ion-transfer process a steady state forward scan voltammogram coupled with a peak-shaped reverse voltammogram could be anticipated. The observation of peak-shaped voltammograms on both forward and reverse indicates that the electroactivity of CAT is not a simple diffusion-controlled process.

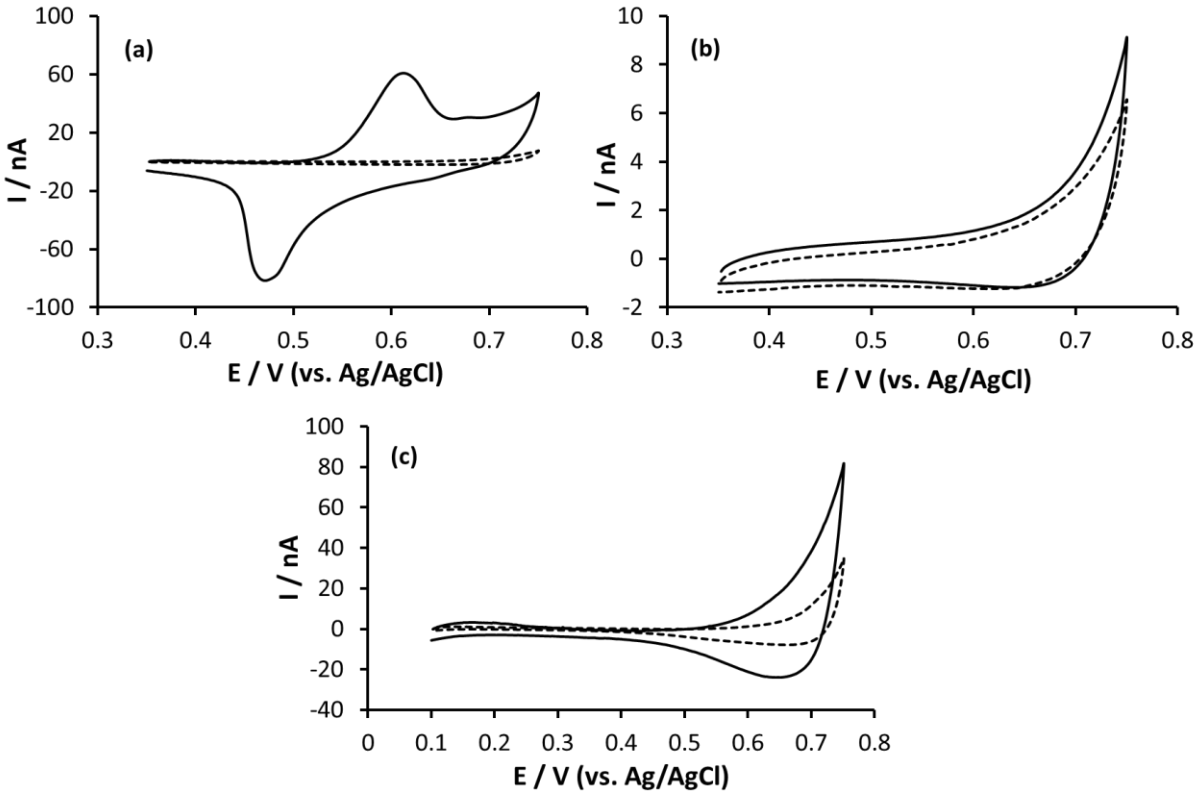

Figure 1. Cyclic voltammetry of CAT at different aqueous phase conditions at the µITIES array (interface formed at laser entry side) (Schematic 1a). CVs recorded for 2 µM CAT in (a: 10 mM HCl, pH 2), (b: 10 mM LiCl, pH 5.5), and 1 µM CAT in (c: 10 mM PBS, pH 7). Scan rate used was 5 mVs^{-1}. Experimental setup used was cell 1 in Schematic 2. In every case 3rd scan of CV were shown.

3.2. Repetitive cyclic voltammetry of CAT under acidic conditions

Figure 2 illustrates the repetitive CVs of 2 µM CAT under acidic conditions which show that the positive and negative peak currents increased with the scan number followed by disappearance of the small post-peak found at potentials positive of the main peak. Some changes observed on repetitive cycling included that the peak current increased with increasing scan number, the main forward peak potential shifted towards higher potentials while, in contrast, the reverse peak potential did not shift with repetitive cycles but the peak current increased gradually, and there was no additional peak found before or after the main peak. In this study the small post-peak was difficult to visualize. After 15-20 scans both the main peak and post-peak merged, in agreement with the behaviour of other proteins [31, 43, 45, 46]. An experiment involving 100 repetitive cycles of 20 µM CAT in 10 mM HCl aqueous phase, following the same approach as used in Figure 2, did not result in deposition of a visible layer at the µITIES, in contrast with studies of lysozyme [46], ferritin [43], haemoglobin [45] or insulin [31]. Despite this, CAT was electroactive at the µITIES and the increase in current up to 15-20 scans indicates that a time-dependent complex process was going on at the interface comprising of a build-up of material and/or adsorption or re-arrangement of CAT at the interface. The increase in current on repeated scans is consistent with formation of a layer of material at the interface, which could occur via protein unfolding or structural changes upon interaction with the interface and/or the anion of the organic phase (as the electroactivity is observed only at pH < pI). The small post-peak might be indicative of structural changes in the early stages of this process, noting that this post-peak is lost on repeated cycling.

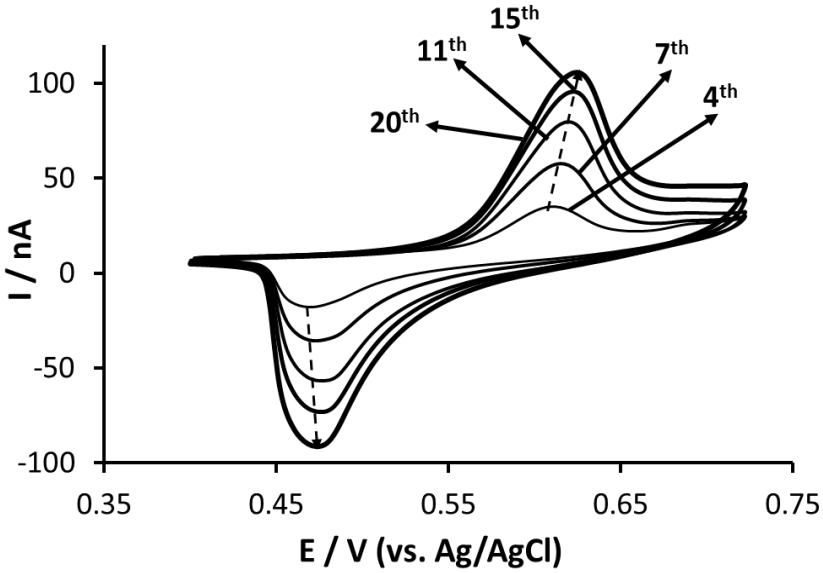

Figure 2. Repetitive cyclic voltammetry of 2 µM CAT at pH 2. CVs were recorded using µITIES array where µinterfaces formed at laser entry side (Schematic 1a). The potential sweep rate was 5 mV s^{-1}. CVs for 4th, 7th, 11th, 15th, and 20th sweeps were selected randomly from repetitive cycles between (1-20)th scans.

3.3. Cyclic voltammetry of increasing concentration of CAT

CVs of increasing concentration of CAT and a calibration curve of peak current versus CAT concentration using cell 1 are displayed in Figure 3. This experiment was carried out at pH 2 using the µITIES array where the micro-interfaces were formed at the laser entry side (the hydrophobic laser entry side, Schematic 1a), i.e. the wider of the pore mouths facing the aqueous phase. With increasing bulk concentration of CAT, both the forward and the reverse peak currents increased linearly with the aqueous phase concentration of CAT. At the lowest CAT concentration studied here, 0.1 µM, the reverse peak at ca. 0.47 V had a peak magnitude of 1.19

± 0.61 nA whilst the forward peak current was 0.40 ± 0.04 nA. With increasing concentration of CAT upto 2 µM, both positive and negative peak currents increased (Figure 3) consistently. In the case of reverse scan, the peak potential did not shift with CAT concentration, but the forward peak potential shifted towards higher potentials. The calibration curve for forward and reverse peak currents showed linear behaviour (R^2 values of 0.9906 and 0.9976, respectively) over the concentration range studied.

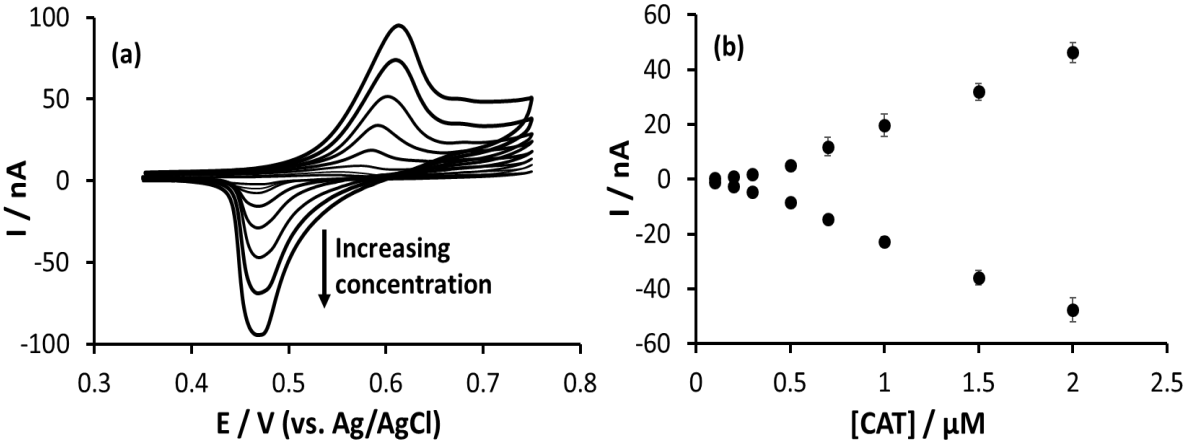

Figure 3. Cyclic votammetry of different concentrations of CAT. (a) CVs (3rd scan of each concentration) of increasing concentration of CAT in the range 0.1 – 2.0 µM using microinterface array where the interfaces are located at laser entry side (Schematic 1a) (b) calibration curve for increasing concentration of CAT by plotting current versus CAT concentration regarding both forward (R^2 = 0.9906) and reverse (R^2 = 0.9976) sweep. Scan rate used was 5 mVs^{-1} . Experimental cell used as depicted in cell 1 (Schematic 2). Each data point is the average of 3 independent measurements; error bars are ±1 standard deviation; where error bars are not visible, they are smaller than the symbol size.

3.4. Scan rate study of CAT

Under acidic aqueous phase conditions (pH 2), a scan rate study was carried out with 2 µM CAT in the range 5-100 mVs^{-1}. At each scan rate, the CV of a single blank (without analyte) was also recorded and then each background response was subtracted from the response in the presence of CAT at that scan rate. The resulting CVs (3rd scan) are displayed in Figure 4. The CV shape is quite dissimilar from that of other proteins (e.g. lysozyme [46], insulin [31], and protamine [47]) where a prewave was observed at the foot of the forward peak, but for CAT electrochemistry a small post-peak was seen, as previously mentioned. With increasing scan rate this post-peak disappeared and merged with the main peak, in a similar manner to that for haemoglobin reported by Herzog *et al.* [45]. The main forward peaks are relatively broad in comparison to the reverse peaks and peak potentials shifted towards higher potential. This broad shape indicates that radial diffusion form the aqueous phase is not the controlling feature of the behaviour, since a steady-state voltammogram would be expected in that case. This behaviour is consistent with the facilitated transfer of the organic phase anion, $TPBCl^-$, across the interface from the organic phase to the aqueous phase. This occurs if positively charged CAT is in close proximity to the interface on the aqueous side. As a result, the forward current may be limited by the diffusion of $TPBCl^-$ in the organic phase held within the microholes of the glass membrane. This facilitation of organic anion transfer depends on the quantity of positively charged CAT present in the aqueous phase due to the much lower concentration of CAT relative to the concentration of $TPBCl^-$ in the organic phase. Most importantly, the scan rate analysis revealed that both the forward and reverse peak currents varied linearly with the square root of scan rate (Figure 4(b & c)), in line with the diffusion of $TPBCl^-$ in the organic phase, towards and away from the interface. In comparison to the forward sweep, a single reverse peak has been found at a lower peak potential with a feature indicative of a desorption process, i.e. a rapid decline in current to background levels after the peak. Despite this feature, the peak current varied linearly with the square root of scan rate indicating a linear diffusion-controlled process. This result also suggests that backward process is controlled by diffusion. Therefore, the CV shape of CAT is suggestive of an adsorption/desorption process, as observed previously [31, 44, 46, 48]. A similar report was presented

by Shinshi *et al.* describing the unusual behaviour of cytochrome c (Cyt c), where controlled-potential electrolysis confirmed the forward scan peak is due to facilitated transfer of supporting electrolyte anion (tetraphenylborate) not by diffusion of Cyt c, and the positive and negative peak currents were proportional to square root of scan rate. These results revealed that Cyt c was not transferred to the organic phase and a diffusion-controlled behaviour due to organic anion transport was observed despite an adsorption/desorption process [48]. Likewise, Amemiya *et al*. showed the transfer of the small protein protamine during the forward scan followed by adsorption at the interface, rather than complete diffusion into the organic phase at micrometer-sized ITIES formed at the tip of a micropipette [47]. As a result, the proposed mechanism of CAT behaviour is that, during the forward scan, positively charged CAT diffuses to the interface and facilitates $TPBCl^-$ transfer from the organic phase to the aqueous phase followed by formation of ion-pair complexes at the aqueous side of the interface. Then the protein/anion complex adsorbs at the interface. A conformational change of CAT molecules might occur after being complexed with $TPBCl^-$ and/or adsorbed at the interface. Finally, during the reverse scan, the complex dissociates with CAT and $TPBCl^-$ returning to their respective phases. The diffusion-controlled processes is diffusion of the anion in the organic phase, where linear diffusion occurs [42]. An alternate mechanism might also describe this phenomenon, where, according to Rosatzin *et al.*, lipophilic borate salts were prone to decompose at low pH [49]. However, reports in the literature employing tetraphenylborate derivatives as organic phase anions in protein electrochemistry at the ITIES do not discuss any degradation of the anions [31, 45, 46, 50]. Although such decomposition might occur, a detailed study is required to investigate this.

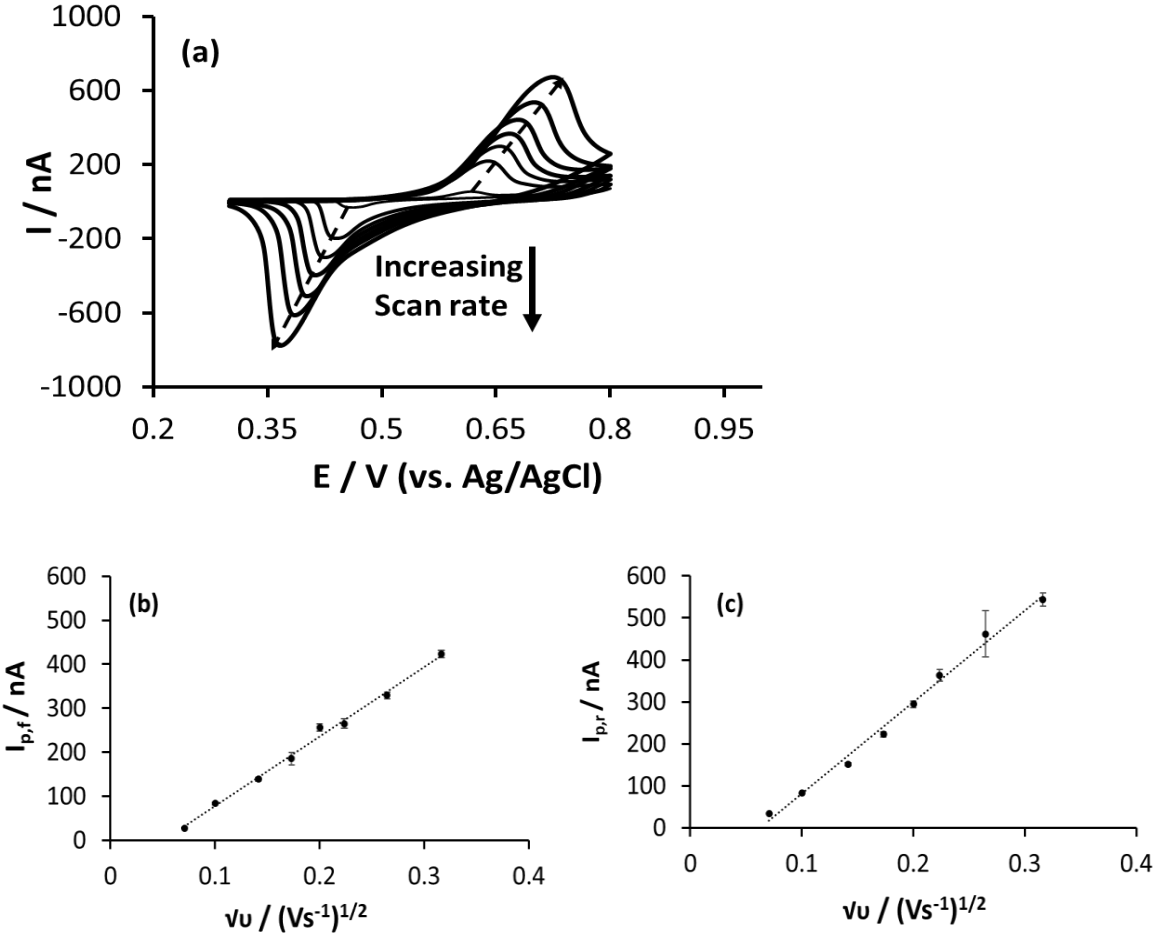

Figure 4. Sweep rate study of CAT. (a) Background subtracted CVs (3rd sweep of each scan rate) of 2 µM CAT at different scan rates at the µITIES array (interfaces formed at laser entry side, Schematic 1a). Electrochemical cell 1. Scan rates: 5, 10, 20, 30, 40, 50, 70, & 100 mVs^{-1}. (b) Plot of forward current versus square root of scan rate, $R^2 = 0.9942$. (c) Plot of reverse current versus square root of scan rate, $R^2 = 0.9921$. Error bars represent ± 1 standard deviation (n = 3).

3.5. Influence of CAT on transfer of TEA^+ at the µITIES array

Following from the previous results, the adsorption/desorption process can be investigated further by conducting CV of a simple ion transfer process in presence of the protein at the µITIES array. It can be inferred that an adsorption process is occuring at the interface in presence of the protein if distortion of the voltammetric response of the simple ion transfer process occurs [44]. Figure 5 shows the CV of 100 µM TEA^+ in presence and absence of CAT in 10 mM HCl aqueous phase. This experiment was done with the array of µinterfaces formed on the laser exit side (i.e. smaller interface size) (Schematic 1b). The black dashed line shows the background CV without any analyte (Figure 5). Within the potential range no background electrolyte transfer occurred. The gray solid line shows the CV when the aqueous phase contained 100 µM TEA^+. The steady-state voltammogram on the forward sweep (positive going) is caused by radial diffusion of TEA^+ ions from the aqueous phase to the organic phase. On the reverse scan, a peak-shaped voltammogram is obtained due to linear diffusion-controlled back transfer of TEA^+ ions from the organic phase to the aqueous phase [42, 44]. The black solid line in Figure 5 shows the CV of 100 µM TEA^+ in presence of 2 µM CAT in aqueous solution. Like other proteins (specifically lysozyme [30] and myoglobin [29]), there was significant distortion of the steady-state and reverse peak currents in presence of CAT. The simple ion transfer should be distorted if the macromolecule adsorbed at the µITIES array depending on the extent of adsorption. The forward steady-state current was completely deformed in the presence of CAT, which indicated that CAT adsorbed at the interface and therefore hampered the free transfer of TEA^+ ions. The reverse peak of TEA^+ was also decreased and less prominent in the presence of CAT in comparison with the voltammogram in the absence of protein. This disruption in steady-state current and decrease in reverse current strongly indicates that CAT is adsorbed at the interface and affected the simple transfer of ions.

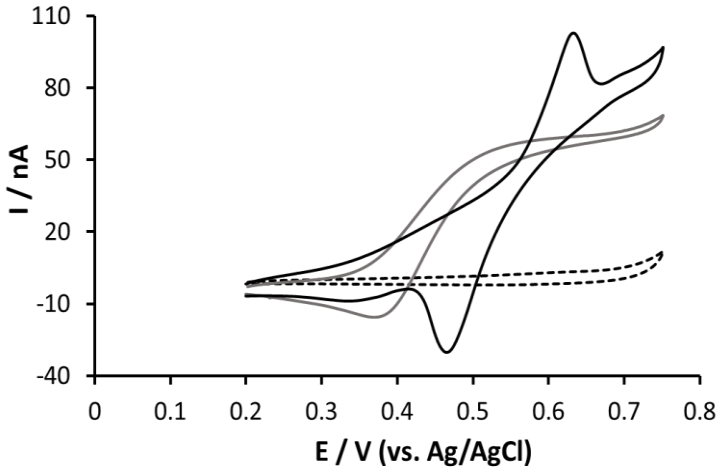

Figure 5. Cyclic voltammetry of CAT in presence of simple ion. CVs of 100 µM tetraethylammonium (TEA^+) in absence (gray solid) and presence of 2 µM CAT (black solid). Aqueous phase was 10 mM HCl (black dashed). Scan rate 5 mV/s. Cell 1 was employed. µITIES array with the hydrophobic laser exit side (Schematic 1b) was used.

3.6. Adsorptive stripping voltammetry of CAT

Adsorptive stripping voltammetry (AdSV) at the µITIES array is a well-known powerful tool for the electroanalysis of a broad range of biomolecules and polyelectrolytes [28, 30, 51]. This technique is usually used to improve the detection limit and analytical sensitivity and is comprised of two major steps: first, at a chosen constant potential, analytes are accumulated or adsorbed onto polarised interface; and second, a voltammetric scan is applied to strip off the accumulated or adsorbed material from the interface and provide an analytical signal [28]. With increasing accumulation or adsorption time, more analyte gets adsorbed at the interface; so the desorptive current recorded on the second step is much higher than the natural conditions where smaller amounts of analyte are naturally present at the interface or adsorbed at the interface. So, sensitivity and detection limits can be enhanced greatly and dependent on the potential and time used to promote analyte adsorption at the interface. To find out the optimized potential to preconcentrate CAT, the effect of applied potential on CAT adsorption was first examined, as reported for lysozyme [30] and haemoglobin [28]. Different potentials were applied for a predetermined adsorption time from higher to

gradually lower positve potentials, and peak currents were recorded on the subsequent scan towards lower potential. On the basis of the maximum peak current obtained from these stripping voltammograms, the most suitable adsorption potential was chosen. As shown in Figure 6, the stripping peak current was dependent on the potential applied during the preconetration step. The optimum applied potential was determined by investigating potentials in the range 0.45 – 0.78 V. Maximum stripping currents obtained in the range 0.6-0.7 V, and the specific potential of 0.68 V provided the largest current, 49.9 ± 3.8 nA, following a 60 s preceoncetration time. The lowest adsorption potnetial at which CAT was detcted was 0.5 V, whereas above 0.68 V, the voltammetric response decreased (Figure 6(b)) due to increased background electrolyte transfer which occurs in this region in the absence of protein [28].

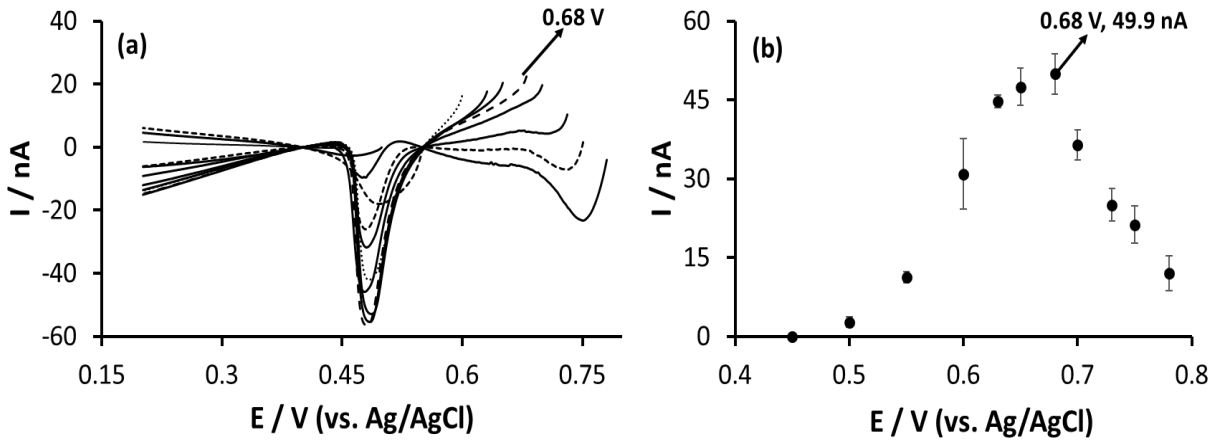

Figure 6. AdSV of 2 µM CAT at different potentials. (a) AdSVs measured at 10 mM HCl using (Cell 1) at different potentials in the range 0.45 V - 0.78 V. µITIES array used with the larger microinterfaces (Schematic 1a) (b) Stripping peak current versus different applied potential. Adsorption time: 60 s, scan rate: 5 mVs^{-1}. Error bars represent ± 1 standard deviation (each data point represents average of 3 separate experiments, n = 3); where error bars are not visible, they are smaller than the symbol size.

The adsorption time also affects the voltammetric response of CAT at the ITIES. To ascertain an optimum adsorption time, an investigation was carried out by applying at a fixed adsorption potential (0.68 V) for different time periods (5 – 480 s) with the same concentration of CAT. Figure 7(a) shows the resulting AdSVs of 2 µM CAT in 10 mM HCl aqueous phase. It can be seen that with increasing preconcentration time, the stripping peak current increased as higher amounts of the cationic protein were adsorbed at the interface and facilitated the transfer of anions from the organic phase across the the interface; the desorptive voltammograms obtained show increased peak current with increased preconcentration time (Figure 7(b)). An adsorption time of 240 s was selected because at longer times the peak current increment was less dramatic and eventually plateaued at longer adsorption times. Again in agreement with the CV results, the AdSV peak shapes reveal a surface-confined process, encompassing the adsorption/desorption phenomenon at the interface.

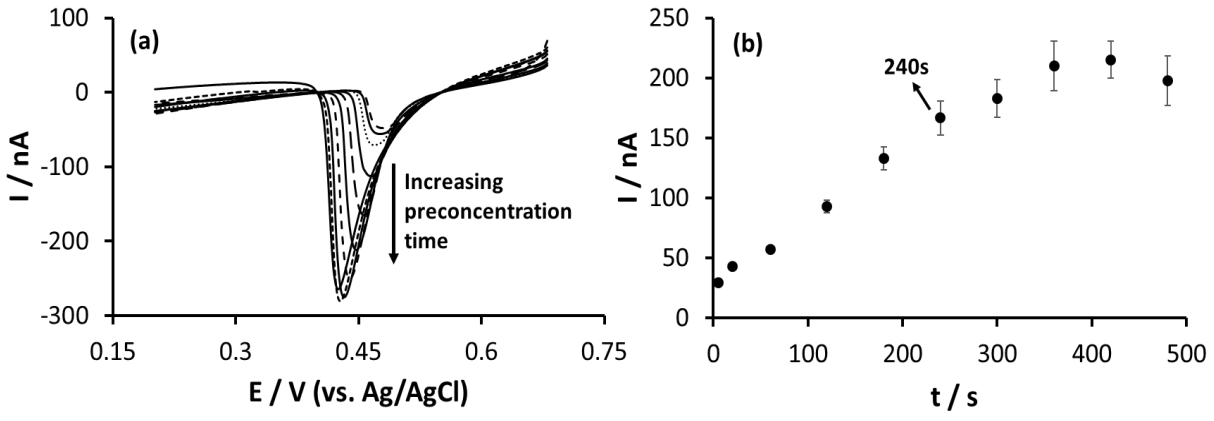

Figure 7. AdSV of 2 μM CAT at different adsorption times. (a) AdSVs were recorded in 10 mM HCl at various adsorption times (5 s to 480 s) for a fixed adsorption potential 0.68 V. (b) Plot of peak current versus adsorption time. Scan rate: 5 mVs^{-1}. μITIES array used was hydrophobic laser entry side (Schematic 1a). Error bars represent ± 1 standard deviation (each data point represents average of 3 separate experiments, n = 3); where error bars are not visible, they are smaller than the symbol size.

3.7. Concentration range for CAT detection

A concentration range of 0.01 – 0.2 μM CAT was examined using a fixed adsorption potential (0.68 V) and adsorption time (240 s). Figure 8(a) shows example voltammograms and Figure 8(b) shows the plot of desorption peak current versus CAT concentration. As can be seen, the peak current did not follow a linear increase with concentration, but presented a hyperbolic increase as also observed with haemoglobin [28] and insulin [52]. After applying an optimized preconcentration time 240 s, the lowest observable and measurable concentration achieved was 0.01 μM (10 nM). The calculated limit of detection was 3.5 nM for a preconcentration time of 240 s. This calculated LOD is based on three times the standard deviation of the response at the lowest concentration divided by the slope of the best-fit straight line through the lowest four concentration points, due to the non-linear response across the full concentration range (Figure 8(b)). This LOD is lower than that reported for lysozyme [30], haemoglobin [28], and insulin [52] using AdSV. It indicates that longer adsorption times can improve the detection capability of biomacromolecules and hence improve the sensitivity. The interfacial concentration of adsorbed protein at the μITIES array was also considered. Surface coverage (Γ) of CAT was calculated using Eq. 1:

$$\Gamma = \frac{Q}{z_i FA} \qquad (1)$$

where Q is charge under the desorption peak (Figure 8(a)) for each concentration studied over 10-200 nM range, z_i is the charge on the protein, presuming at pH 2, it would carry +80 charges, F is the Faraday constant (96485 C mol^{-1}), A is the total geometric area of the μinterface array (13.85×10^{-4} cm^2), and Γ is the surface coverage (mol cm^{-2}). At 240 s preconcentration time, the charges under the desorption peak corresponds to surface coverages in the range 0.001- 0.102 pmol cm^{-2} over the above mentioned concentration range. Taking into account the size of CAT, (r_h, hydrodynamic radius of CAT is 5.2 nm) [7], its monolayer surface coverage is estimated to be 1.70 pmol cm^{-2}. As a result, the experimental surface coverages determined from the AdSV voltammograms correspond to sub-monolayers at the interface: the maximum concentration studied (200 nM) yielded a surface coverage of ca. 0.05 monolayer.

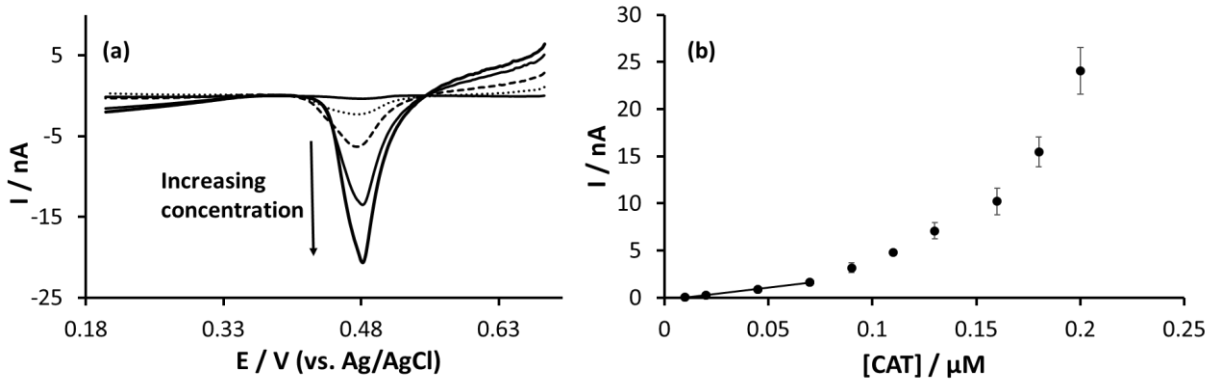

Figure 8. AdSV of increasing concentration of 0.01-0.2 μM CAT. (a) AdSVs were measured at 10 mM HCl upon application of initial optimized potential 0.68 V for the duration of 240s preconcentration time. AdSVs for only five of the concetrations studied (0.02, 0.09, 0.13, 0.18, and 0.2) μM are displayed here. (b) Calibration curve of desorptive peak current versus CAT concentration. Scan rate: 5 mVs^{-1}, electrochemical cell 1, μITIES used (Schematic 1a). Error bars represent ± 1 standard deviation (n = 3); where error bars are not visible, they are smaller than the symbol size.

3.8. Cyclic voltammetry of CAT in artificial serum

As an indication of possible matrix effects for analytical applications of the electrochemical behaviour of CAT at a µITIES array, experiments were undertaken with an aqueous phase of artificial serum (AS) solution. CV of CAT was carried out in AS sample at three different pH values (2.64, 4.95 and 7.44) to indicate whether any interference may arise from these matrices that might impact the analytical response of CAT itself. AS was prepared following published compositions [53, 54]. Figure 9(a) displays a CV with the artificial serum as the aqueous phase without the presence of CAT. When AS was compared with other pure aqueous electrolyte solutions (e.g. 10 mM LiCl, 10 mM HCl), its potential window was shorter due to the presence of various ionic species which transfer at lower potentials, in agreement with previous findings [53]. This result also supports the findings from a study of synthetic urine where it has been shown that NH_4^+, K^+, and Ca^{2+} are responsible for the shorter potential window [51]. Three different pH values were examined to see the effect on the electrochemical behaviour of CAT when AS was employed as the working matrix. A background-subtracted CV of 1.4 µM CAT is shown in Figure 9(b) where the aqueous phase (AS) pH was 2.64 and a characteristic voltammogram with forward and reverse peaks was recorded which was in contrast to that at pH 4.95, where the forward peak was not clear but a pronounced reverse peak was recorded at 0.6 V (Figure 9(c)). So, at pH values lower than pI, CAT is detectable in AS as also observed in regular electrolyte solution. At pH 7.44, in AS adjusted with 10 mM LiOH solution, no sharp reverse peak response was recorded (Figure 9(d)) which is because at pH 7.44, CAT is anionic in nature and not detectable by the anion-facilitated response that occurs at pH values lower than the pI.

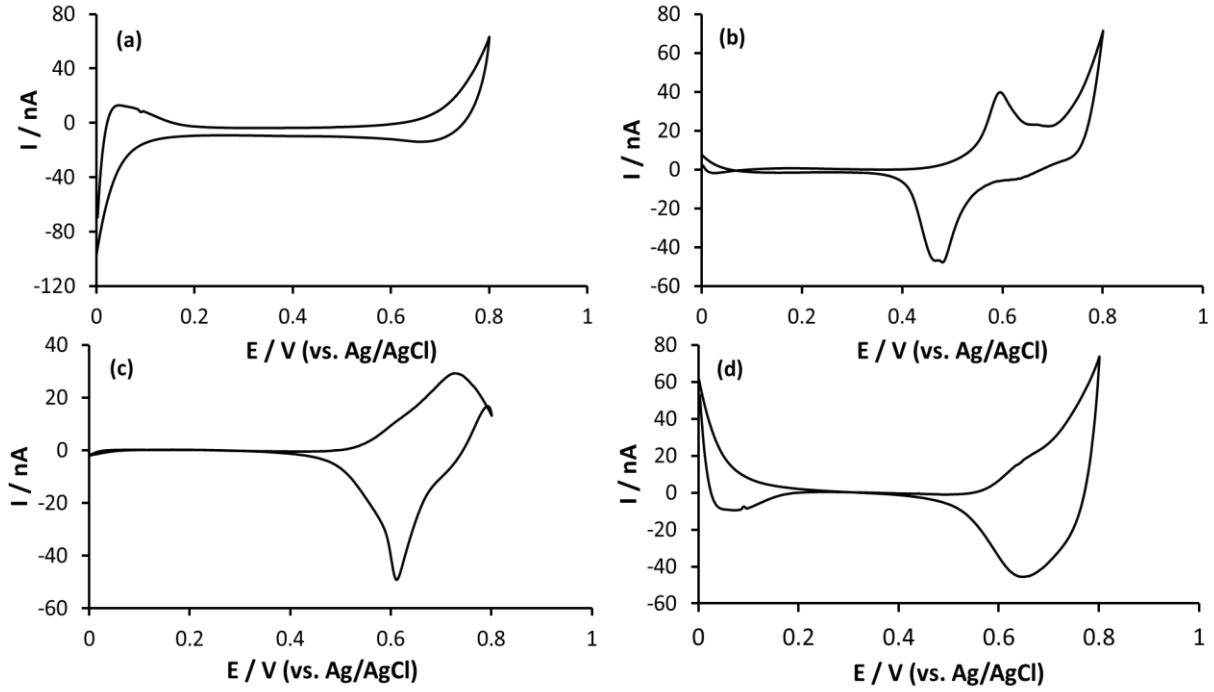

Figure 9. Cyclic voltammetry of artificial serum at different pH conditions in presence and absence of CAT. (a) CV of artificial serum (pH 4.95) without analyte. Background subtracted CVs of (b) 1.4 µM CAT (3rd run) in AS (pH 2.64 adjusted by 10 mM HCl (c) 2 µM CAT (3rd run) in AS (pH 4.95), and (d) 2 µM CAT (3rd run) in AS (pH 7.44 adjusted by 10 mM LiOH). Scan rate used was 5 mV/s at the µITIES array (hydrophobic laser entry side) (Schematic 1a). Electrochemical cell 1 was used.

Depending on the repetitive sweeps, the CVs of CAT varied as discussed before. Figure S2 shows repetitive CVs in AS at different pH values. The CV of CAT in AS at pH 2.64 provided comprehensible forward and reverse peaks which increased in magnitude with successive scans even in such complex electrolyte compositions (Figure S2(a)). At pH 4.95, no obvious reverse peak was recorded on the 1st scan but on the 3rd and 8th scans a noticeable reverse peak was seen (Figure S2(b)). At pH higher than the pI, some small changes were noticed. No clear reverse peak was detected on the 1st and 3rd scans but on higher scan numbers, a reverse peak appeared which might indicate some interactions between the anionic protein and the electrolyte cations present in AS (Figure S2(c)). Such behaviour might also be anticipated for the electrochemistry of CAT within biological samples hence an interesting possibility for detection at more physiologically-relevant pH values.

4. Conclusion

Catalase electrochemistry has been investigated at an liquid-liquid micro-interface array by cyclic voltammetry and adsorptive stripping voltammetry. CVs revealed an electrochemical behaviour with distinct forward and reverse peaks suggesting an adsorption/desorption process at the interface accompanied by formation of ion-pair complex between the cationic CAT and anions of organic electrolyte phase, despite the scan rate study suggesting a diffusion-controlled process. No voltammetric response was found at pH > pI, so that CAT is only electroactive at the ITIES when it is positively charged. The reverse peak in CV and stripping peak in AdSVs present a desorption phenomenon as a sharp decline in current magnitude to the background level, similar to previously observed behaviour for lysozyme, myoglobin, haemoglobin and insulin. Adsorptive stripping voltammetry was carried out to assess the sensitivity and improve the detection limit. It has been found that at 0.68 V preconcentration potential promoted maximum CAT adsorption at the interface and a minimum of 0.01 µM concentration was detected following 240 s preconcentration; the calculated LOD (3.5 nM) was lower than that for other proteins at the ITIES reported to-date. It might be possible to push the LOD of CAT to lower concentrations employing differential pulse voltammetry in combination with AdSV at µITIES arrays. The cyclic voltammogram study of CAT in artificial serum (at pH 2.64 & pH 4.95) revealed that it is detectable even in complex serum matrix despite the presence of various ionic species. But extensive study required to prove this assumption as the source of CAT was from bovine, not from human. Further study needs to be carried out to varify the human CAT. The results found in this study suggest the attainability of elctrochemical techniques as an analytical device for the detection of CAT as it is considered as a biomarker without any labelling at the L/L µinterface array. For employing this technique in practical application (e.g., biosensor development) further investigation required.

Acknowledgements

SZ thanks Curtin University for the award of an Australian Government Research Training Programme Scholarship. We thank a reviewer for comments about a possible alternative mechanism.

References

[1] M.R.N. Murthy, T.J. Reid, A. Sicignano, N. Tanaka, M.G. Rossmann, Structure of beef liver catalase, Journal of Molecular Biology, 152 (1981) 465-499.

[2] H.-J. Jiang, H. Yang, D.L. Akins, Direct electrochemistry and electrocatalysis of catalase immobilized on a SWNT-nanocomposite film, Journal of Electroanalytical Chemistry, 623 (2008) 181-186.

[3] L.H. Johansson, L.A. Håkan Borg, A spectrophotometric method for determination of catalase activity in small tissue samples, Analytical Biochemistry, 174 (1988) 331-336.

[4] I. Fita, M.G. Rossmann, The NADPH binding site on beef liver catalase, Proc Natl Acad Sci U S A, 82 (1985) 1604-1608.

[5] A. Díaz, P.C. Loewen, I. Fita, X. Carpena, Thirty years of heme catalases structural biology, Archives of Biochemistry and Biophysics, 525 (2012) 102-110.

[6] B.L. Nannenga, D. Shi, J. Hattne, F.E. Reyes, T. Gonen, Structure of catalase determined by MicroED, Elife, 3 (2014) e03600-e03600.

[7] H.P. Erickson, Size and shape of protein molecules at the nanometer level determined by sedimentation, gel filtration, and electron microscopy, Biol Proced Online, 11 (2009) 32-51.

[8] W.A. Schroeder, J.R. Shelton, J.B. Shelton, B.M. Olson, Some amino acid sequences in bovine-liver catalase, Biochimica et Biophysica Acta (BBA) - Specialized Section on Enzymological Subjects, 89 (1964) 47-65.

[9] T. Samejima, M. Kamata, K. Shibata, Dissociation of Bovine Liver Catalase at Low pH, The Journal of Biochemistry, 51 (1962) 181-187.

[10] N. Seetharamaiah, N. Seetharamaiah, N. Pathappa, S.M. Jose, S.S. Gurukar, Metal-ion co-ordination assembly based multilayer of one dimensional gold nanostructures and catalase as electrochemical sensor for the analysis of hydrogen peroxide, Sensors and Actuators B: Chemical, 245 (2017) 726-740.

[11] A.L. Brioukhanov, A.I. Netrusov, R.I.L. Eggen, The catalase and superoxide dismutase genes are transcriptionally up-regulated upon oxidative stress in the strictly anaerobic archaeon Methanosarcina barkeri, Microbiology, 152 (2006) 1671-1677.

[12] W. Hansberg, R. Salas-Lizana, L. Domínguez, Fungal catalases: Function, phylogenetic origin and structure, Archives of Biochemistry and Biophysics, 525 (2012) 170-180.

[13] L. Góth, P. Rass, A. Páy, Catalase enzyme mutations and their association with diseases, Molecular Diagnosis, 8 (2004) 141-149.

[14] J. Kodydková, L. Vávrová, M. Kocík, A. Žák, Human catalase, its polymorphisms, regulation and changes of Its activity in different diseases, Folia Biologica (Czech Republic), 60 (2014) 153-167.

[15] C. Glorieux, M. Zamocky, J.M. Sandoval, J. Verrax, P.B. Calderon, Regulation of catalase expression in healthy and cancerous cells, Free Radical Biology and Medicine, 87 (2015) 84-97.

[16] D.G. Bostwick, E.E. Alexander, R. Singh, A. Shan, J. Qian, R.M. Santella, L.W. Oberley, T. Yan, W. Zhong, X. Jiang, T.D. Oberley, Antioxidant enzyme expression and reactive oxygen species damage in prostatic intraepithelial neoplasia and cancer, Cancer, 89 (2000) 123-134.

[17] G.F. Gaetani, A.M. Ferraris, M. Rolfo, R. Mangerini, S. Arena, H.N. Kirkman, Predominant role of catalase in the disposal of hydrogen peroxide within human erythrocytes, Blood, 87 (1996) 1595-1599.

[18] N.S.F. Ramli, S. Mat Junit, N.K. Leong, N. Razali, J.J. Jayapalan, A. Abdul Aziz, Analyses of antioxidant status and nucleotide alterations in genes encoding antioxidant enzymes in patients with benign and malignant thyroid disorders, PeerJ, 5 (2017) e3365-e3365.

[19] L. Wang, J. Wang, F. Zhou, Direct Electrochemistry of Catalase at a Gold Electrode Modified with Single-Wall Carbon Nanotubes, Electroanalysis, 16 (2004) 627-632.

[20] M.E. Lai, A. Bergel, Direct electrochemistry of catalase on glassy carbon electrodes, Bioelectrochemistry, 55 (2002) 157-160.

[21] G. Herzog, Recent developments in electrochemistry at the interface between two immiscible electrolyte solutions for ion sensing, Analyst, 140 (2015) 3888-3896.

[22] Z. Samec, Electrochemistry at the interface between two immiscible electrolyte solutions (IUPAC Technical Report), Pure and Applied Chemistry, 2004, pp. 2147.

[23] S. Liu, Q. Li, Y. Shao, Electrochemistry at micro- and nanoscopic liquid/liquid interfaces, Chemical Society Reviews, 40 (2011) 2236-2253.

[24] B. Liu, M.V. Mirkin, Electrochemistry at Microscopic Liquid–Liquid Interfaces, Electroanalysis, 12 (2000) 1433-1446.

[25] C.A. Morris, A.K. Friedman, L.A. Baker, Applications of nanopipettes in the analytical sciences, Analyst, 135 (2010) 2190-2202.

[26] M.V. Colqui Quiroga, L.M.A. Monzón, L.M. Yudi, Interaction of triflupromazine with distearoylphosphatidylglycerol films studied by surface pressure isotherms and cyclic voltammetry at a 1,2-dichloroethane/water interface, Electrochimica Acta, 55 (2010) 5840-5846.

[27] H. Tatsumi, T. Ueda, Ion transfer voltammetry of tryptamine, serotonin, and tryptophan at the nitrobenzene/water interface, Journal of Electroanalytical Chemistry, 655 (2011) 180-183.

[28] E. Alvarez De Eulate, L. Serls, D.W.M. Arrigan, Detection of haemoglobin using an adsorption approach at a liquid-liquid microinterface array, Analytical and Bioanalytical Chemistry, 405 (2013) 3801-3806.

[29] S. O'Sullivan, D.W.M. Arrigan, Electrochemical behaviour of myoglobin at an array of microscopic liquid-liquid interfaces, Electrochimica Acta, 77 (2012) 71-76.

[30] E. Alvarez de Eulate, D.W.M. Arrigan, Adsorptive Stripping Voltammetry of Hen-Egg-White-Lysozyme via Adsorption–Desorption at an Array of Liquid–Liquid Microinterfaces, Analytical Chemistry, 84 (2012) 2505-2511.

[31] F. Kivlehan, Y.H. Lanyon, D.W.M. Arrigan, Electrochemical study of insulin at the polarized liquid-liquid interface, Langmuir, 24 (2008) 9876-9882.

[32] T. Osakai, Y. Yuguchi, E. Gohara, H. Katano, Direct Label-free Electrochemical Detection of Proteins Using the Polarized Oil/Water Interface, Langmuir, 26 (2010) 11530-11537.

[33] L. Poltorak, N. van der Meijden, S. Oonk, E.J.R. Sudhölter, M. de Puit, Acid phosphatase behaviour at an electrified soft junction and its interfacial co-deposition with silica, Electrochemistry Communications, 94 (2018) 27-30.

[34] M.D. Scanlon, G. Herzog, D.W.M. Arrigan, Electrochemical detection of oligopeptides at silicon-fabricated micro-liquid|liquid interfaces, Analytical Chemistry, 80 (2008) 5743-5749.

[35] L. Poltorak, N. van der Meijden, S. Skrzypek, E.J.R. Sudhölter, M. de Puit, Co-deposition of silica and proteins at the interface between two immiscible electrolyte solutions, Bioelectrochemistry, 134 (2020) 107529.

[36] R.S. Vasan, Biomarkers of cardiovascular disease: Molecular basis and practical considerations, Circulation, 113 (2006) 2335-2362.

[37] D. Anderson, WHO task group on environmental health criteria for biomarkers in risk assessment: Validity and validation members, Environmental Health Criteria, 2001, pp. XI-XX.

[38] R.A. Bradshaw, H. Hondermarck, H. Rodriguez, Cancer Proteomics and the Elusive Diagnostic Biomarkers, PROTEOMICS, 19 (2019) 1800445.

[39] D.N. Cagney, J. Sul, R.Y. Huang, K.L. Ligon, P.Y. Wen, B.M. Alexander, The FDA NIH Biomarkers, EndpointS, and other Tools (BEST) resource in neuro-oncology, Neuro Oncol, 20 (2018) 1162-1172.

[40] S.N. Topkaya, M. Azimzadeh, M. Ozsoz, Electrochemical Biosensors for Cancer Biomarkers Detection: Recent Advances and Challenges, Electroanalysis, 28 (2016) 1402-1419.

[41] R. Akter, D.W.M. Arrigan, Detection of prostate specific membrane antigen at picomolar levels using biocatalysis coupled to assisted ion transfer voltammetry at a liquid-organogel microinterface array, Analytical Chemistry, 88 (2016) 11302-11305.

[42] E. Alvarez de Eulate, J. Strutwolf, Y. Liu, K. O'Donnell, D.W.M. Arrigan, An Electrochemical Sensing Platform Based on Liquid–Liquid Microinterface Arrays Formed in Laser-Ablated Glass Membranes, Analytical Chemistry, 88 (2016) 2596-2604.

[43] H. Sakae, Y. Toda, T. Yokoyama, Electrochemical behavior of ferritin at the polarized water|1,2-dichloroethane interface, Electrochemistry Communications, 90 (2018) 83-86.

[44] M.D. Scanlon, J. Strutwolf, D.W.M. Arrigan, Voltammetric behaviour of biological macromolecules at arrays of aqueous|organogel micro-interfaces, Physical Chemistry Chemical Physics, 12 (2010) 10040-10047.

[45] G. Herzog, V. Kam, D.W.M. Arrigan, Electrochemical behaviour of haemoglobin at the liquid/liquid interface, Electrochimica Acta, 53 (2008) 7204-7209.

[46] M.D. Scanlon, E. Jennings, D.W.M. Arrigan, Electrochemical behaviour of hen-egg-white lysozyme at the polarised water/1, 2-dichloroethane interface, Physical Chemistry Chemical Physics, 11 (2009) 2272-2280.

[47] S. Amemiya, X. Yang, T.L. Wazenegger, Voltammetry of the Phase Transfer of Polypeptide Protamines across Polarized Liquid/Liquid Interfaces, Journal of the American Chemical Society, 125 (2003) 11832-11833.

[48] M. Shinshi, T. Sugihara, T. Osakai, M. Goto, Electrochemical extraction of proteins by reverse micelle formation, Langmuir, 22 (2006) 5937-5944.

[49] T. Rosatzin, E. Bakker, K. Suzuki, W. Simon, Lipophilic and immobilized anionic additives in solvent polymeric membranes of cation-selective chemical sensors, Analytica Chimica Acta, 280 (1993) 197-208.

[50] A. Trojánek, J. Langmaier, E. Samcová, Z. Samec, Counterion binding to protamine polyion at a polarised liquid–liquid interface, Journal of Electroanalytical Chemistry, 603 (2007) 235-242.

[51] B.M.B. Felisilda, A.D. Payne, D.W.M. Arrigan, Electrochemical Behavior and Detection of Sulfated Sucrose at a Liquid|Organogel Microinterface Array, Analytical Chemistry, 90 (2018) 10256-10262.

[52] S. O'Sullivan, E. Alvarez de Eulate, Y.H. Yuen, E. Helmerhorst, D.W.M. Arrigan, Stripping voltammetric detection of insulin at liquid–liquid microinterfaces in the presence of bovine albumin, Analyst, 138 (2013) 6192-6196.

[53] C.J. Collins, C. Lyons, J. Strutwolf, D.W.M. Arrigan, Serum-protein effects on the detection of the β-blocker propranolol by ion-transfer voltammetry at a micro-ITIES array, Talanta, 80 (2010) 1993-1998.

[54] M. Cretin, L. Alerm, J. Bartroli, P. Fabry, Lithium determination in artificial serum using flow injection systems with a selective solid-state tubular electrode based on NASICON membranes, Analytica Chimica Acta, 350 (1997) 7-14.